ENVIRONMENTAL STUDIES

# Plastic degradation by insect hexamerins: Near-atomic resolution structures of the polyethylene-degrading proteins from the wax worm saliva

**Mercedes Spínola-Amilibia[1], Ramiro Illanes-Vicioso[2], Elena Ruiz-López[2], Pere Colomer-Vidal[3], Francisco Ventura Rodriguez[3], Rosa Peces Pérez[3], Clemente F. Arias[3,4], Tomas Torroba[5], Maria Solà[2]*, Ernesto Arias-Palomo[1]*, Federica Bertocchini[3]***



**Plastic waste management is a pressing ecological, social, and economic challenge. The saliva of the lepidopteran *Galleria mellonella* larvae is capable of oxidizing and depolymerizing polyethylene in hours at room temperature. Here, we analyze by cryo–electron microscopy (cryo-EM) *G. mellonella*'s saliva directly from the native source. The three-dimensional reconstructions reveal that the buccal secretion is mainly composed of four hexamerins belonging to the hemocyanin/phenoloxidase family, renamed Demetra, Cibeles, Ceres, and a previously unidentified factor termed Cora. Functional assays show that this factor, as its counterparts Demetra and Ceres, is also able to oxidize and degrade polyethylene. The cryo-EM data and the x-ray analysis from purified fractions show that they self-assemble primarily into three macromolecular complexes with striking structural differences that likely modulate their activity. Overall, these results establish the ground to further explore the hexamerins' functionalities, their role in vivo, and their eventual biotechnological application.**

## INTRODUCTION

Plastic utilization has generated millions of tons of residues that have been polluting our environment since the second half of the 20th century. The most produced and resistant plastic polymers, polyethylene (PE), polypropylene (PP), polystyrene (PS), and polyvinyl chloride (PVC), account for 70% of total global plastic production (*1*). These residues keep accumulating in any niche of the planet. Finding an environmental sustainable solution has become a priority among the various challenges human kind is bound to face in this 21st century. Mechanical recycling, the recycling technology mostly used so far, has been proved to be highly inefficient and ineffective (*2*–*4*). In the absence of better alternatives, plastic residues are either incinerated or disposed of into landfill sites.

In the past two decades, an emerging field started raising hopes of a way to manage plastic residues, which is degradation by biological means. One of these means, known as biodegradation, relies on the capacity of microorganisms to break down plastic and metabolize it (*5*–*8*). However, the ability of biological systems to degrade plastics is not restricted to microorganisms. The capacity of some Coleoptera and Lepidoptera larvae to break down PE and PS opened the door to the use of insects as potential plastic degraders (*9*–*20*). The fastest insects known to date are the larvae of lepidopteran *Galleria mellonella*, also known as wax worm (ww), which are able to chemically modify PE by oxidizing the polymer within a few hours from exposure at room temperature (*12*, *21*). Since the first studies on the larvae of lepidopteran *Plodia interpunctella* and coleopteran *Tenebrio molitor* (*9*–*11*), efforts have been concentrated on the microbiome residing in the larvae's gut, with the idea that only microorganisms are capable of breaking down sturdy plastics as a result of their metabolic activity (*9*, *10*, *14*–*17*, *19*, *22*). Despite the intense effort in this direction, the data collected so far resulted inconclusive, and doubts have been shed on the primary role of microorganisms in the insect larvae's ability (*13*, *23*). In this line, recent studies further questioned a primary role of the invertebrates' microbiome (*24*), showing that the larvae of *G. mellonella* oxidize PE using their own saliva, defined as the liquid collected from the buccal opening (*21*). In particular, proteins of the hexamerin family present in the insect saliva proved to oxidize PE. The fact that these proteins are produced by the very same invertebrate confirmed the ww as the primary cause of PE degradation (*21*).

The discovery that the ww capability to oxidize and degrade PE resides in their saliva and, particularly, in some of the proteins therein contained laid the foundation of a new paradigm of plastic degradation by biological means. The oxidation of the polymer is widely recognized as the critical initial step in the degradation of plastics. This resistance to oxidation is a purposely designed feature responsible for plastic durability. While microorganism can metabolize the short oxidized molecules deriving from the environmental plastic degradation, the initial step of this process, namely, the introduction of oxygen within the polymeric structure, is the most problematic one. The ww hexamerins can provide a fundamental complement or a potential alternative to the currently available strategies of plastic degradation by biological means, which rely on aggressive abiotic pretreatments to overcome the oxidation step (*7*, *25*). Keys in the understanding of this capability are the exact composition and molecular organization of these ww factors in the saliva, which remain unknown to date.

To address these issues, we performed cryo–electron microscopy (cryo-EM) analyses directly on native saliva samples. The three-

[1]Department of Structural and Chemical Biology, Centro de Investigaciones Biológicas Margarita Salas, CSIC, 28040 Madrid, Spain. [2]Department of Structural Biology, Molecular Biology Institute of Barcelona (IBMB), CSIC, Barcelona Science Park, 08028 Barcelona, Spain. [3]Department of Plant and Microbial Biology, Centro de Investigaciones Biológicas Margarita Salas, CSIC, 28040 Madrid, Spain. [4]Grupo Interdisciplinar de Sistemas Complejos, GISC, Madrid, Spain. [5]Department of Chemistry, Faculty of Science and PCT, University of Burgos, Burgos, Spain.
*Corresponding author. Email: maria.sola@ibmb.csic.es (M.S.); earias@cib.csic.es (E.A.-P.); federicona@hotmail.com (F.B.)

dimensional (3D) classification of the cryo-EM particles confirmed the presence in the saliva of three previously identified hexamerins (*21*), together with another protein belonging to the same family. One of these proteins, a methionine-rich hexamerin, is capable of oxidizing PE. Analogously to the previously identified hexamerins, treating PE with this protein at room temperature resulted in the oxidation of the polymer and the formation of degradation products after a few hours of exposure.

The combined cryo-EM and crystallography data presented here show that these hexamerins exhibit striking disparities in their relative abundance, distinct posttranslational modifications, and major structural differences in their metal-binding sites. Furthermore, the ww hexamerins do not seem to share a canonical well-defined active site equivalent to that found in the related hemocyanins (Hcs) and phenoloxidases (POs). Such a high degree of structural divergence is in stark contrast with that of PETases, the only other enzymes, to date, capable of degrading a synthetic polymer [polyethylene terephthalate (PET)] (*26*–*30*). Despite the heterogeneous sources of PETases, their catalytic site is almost completely conserved (*31*).

Our results reveal a much more complex landscape for the ww hexamerins, where the structure/function relationship appears to be more convoluted, and set the ground to characterize the precise role of this poorly understood family of proteins. Collectively, the cryo-EM and x-ray analyses provide the high-resolution structures of the main proteins present in *G. mellonella*'s saliva and represent a necessary and promising launching point to explore the emerging field of PE degradation by insect proteins.

## RESULTS

This section is structured as follows. A general description of the saliva biological sample is followed by a detailed structural description of each of the identified protein complexes (Demetra/Cibeles heterohexamer, Ceres homohexamer, and Cora homohexamer). Last, a description of Cora activity on PE is presented.

### Cryo-EM analysis reveals the molecular organization and composition of the main proteins found in *G. mellonella*'s saliva

A recent study showed that the PE-degrading activity of *G. mellonella*'s saliva is associated with the protein fraction of the buccal secretion (*21*). Mass spectrometry (MS) data revealed that this fraction contains a mix of proteins that belong to the hexamerin/PO superfamily (*21*). Given the high molecular mass of the complexes formed by this type of proteins, we directly analyzed the buccal secretion by cryo-EM as an initial step to understand the 3D architecture and nature of such plastic-degrading factors. The cryo-EM micrographs showed clean particles with good contrast (Fig. 1). In addition, the initial reconstructions showed that the overall dimensions (~120 Å × 120 Å × 90 Å) were consistent with previous gel filtration data that suggested large particle dimensions (~450 kDa) (*21*), and with the typical molecular organization of most members of the hexamerin/PO superfamily (Fig. 1).

During treatment of the cryo-EM data, the initial attempts to separate the different classes of protein particles present in the saliva sample were challenging due to their overall structural similarity. However, after several rounds of 3D classification, the quality of the images allowed us to determine that the particles could be divided into three distinct populations (Fig. 1, fig. S1, and table S1). The three reconstructions finally converged at 2.3, 2.8, and 1.9 Å (fig. S2), which allowed us to model the corresponding polypeptide chains in the EM maps and unambiguously identify the sequence of the proteins (Fig. 1).

Thus, sequencing based on the cryo-EM maps clearly showed four subpopulations composed of different proteins. Since the identification codes of these proteins are complex and nonintuitive, and in addition their specific natural function and the reaction they catalyze is completely unknown, no activity-related name could be assigned. Therefore, we decided to rename them following a previous work (*21*), the name hereby indicated in brackets. The first subpopulation was composed of a heterocomplex formed by XP_026756396 (Demetra) (*21*) and a closely related protein (81% sequence identity) g18163 or XP_026756460 (Cibeles) (*21*). The second group corresponded to the hexamerin aJHSP1, XP_026756459 (Ceres) (*21*), and finally, in the third reconstruction, we identified a methionine-rich protein bJHSP1, XP_026749149 (Cora). Two of these hexamerins (Demetra and Ceres) have been shown to oxidize and degrade PE (*21*).

All four proteins share a substantial sequence similarity (~30 to 32% sequence identity; see Fig. 2, A and B, for details) and belong to the hexamerin family, which is part of a larger superfamily that includes groups of proteins with distantly related functions, such as the oxygen carrier Hcs, pseudo-Hcs, and POs (*32*). The monomers of the hexamerin family present a characteristic 3D fold, conserved in the four proteins described here, which consist of an α-helical N-terminal region (Fig. 2C), a middle subdomain, and an immunoglobulin (Ig)–like C-terminal region rich in ß strands (these domains are normally referred to as Hc-N, Hc-M, and Hc-C, which stand for Hc N-terminal, middle, and C-terminal domains, respectively) (Fig. 2C) (*33*, *34*). The central subdomain in Hcs and POs contains a di-copper active site rich in histidines, responsible for oxygen binding (Hc) and other enzymatic activities (PO). In contrast, such a conserved catalytic site is absent in all hexamerins, including the four proteins hereby described (Fig. 2C). Typically, these ~78-kDa monomers self-assemble into hetero- or homohexamers formed by two trimeric rings organized back to back in a staggered configuration (i.e., a monomer docks into the crevice formed between two monomers of the opposing ring) (Fig. 2C). Overall, the cryo-EM analysis revealed that the saliva of the insect larva contains four hexamerins that self-assemble into three main oligomers and confirmed that the sequence of the family active site is not conserved.

### The mature forms of Demetra and Cibeles self-associate predominantly into a 3:3 heterocomplex

During the early steps of image processing (Fig. 1 and fig. S1), the first group of particles (152,240) appeared to contain identical monomers, forming a homohexamer, and thus have D3 symmetry. Although the density of the EM map matched the sequence of Cibeles considerably well, some areas of the reconstruction suggested that it could contain a mixture of different molecules. Initial 3D classification attempts were not successful and the heterogeneity could only be resolved after processing the data using symmetry relaxation [as implemented in (*35*, *36*)]. This procedure revealed that more than 50% of the analyzed particles actually had C3 symmetry, with clear differences between the two trimeric rings, and determined that Cibeles and Demetra mainly formed a 3:

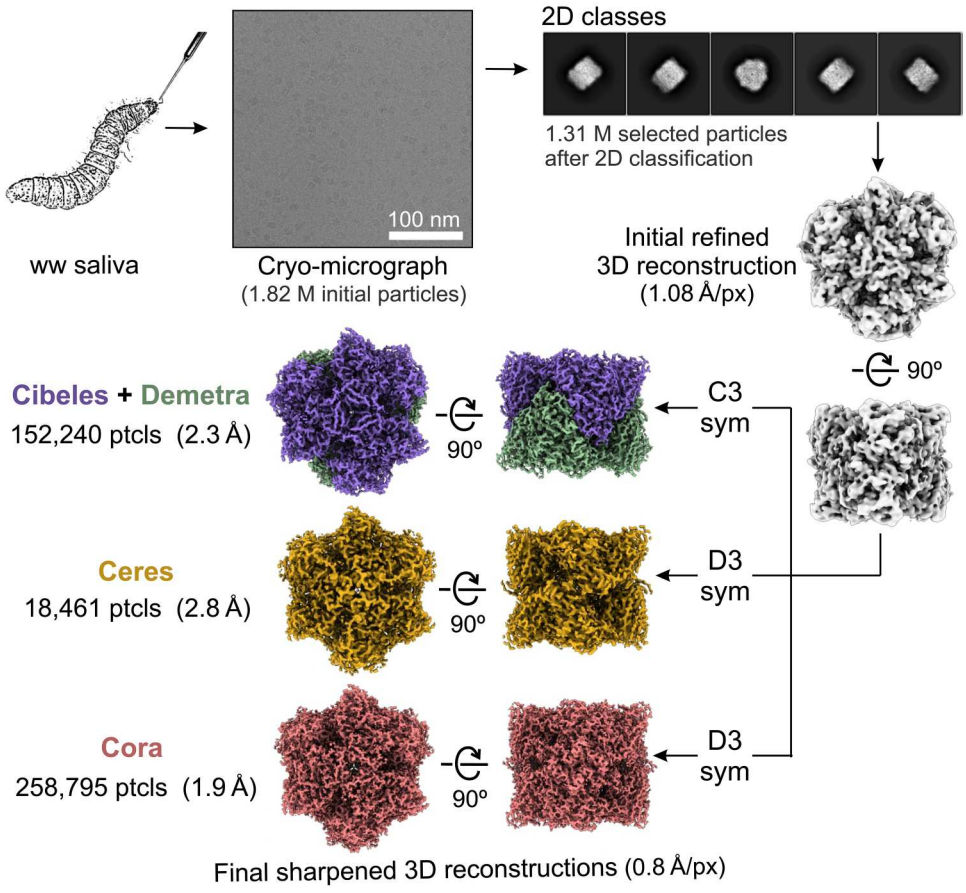


**Fig. 1. Cryo–electron microscopy (cryo-EM) analysis of *G. mellonella* saliva.** The saliva was diluted and directly applied to carbon-coated cryo-EM grids. Single-particle analysis revealed that wax worm (ww) buccal secretion is composed of three main oligomeric complexes formed by four proteins. ptcls, particles; sym, symmetry.

heterohexamer (molecules A, B, C, and D, E, F, respectively; Fig. 3, A and B and fig. S1).

The final 2.3 Å resolution map (Fig. 1 and fig. S1) allowed us to model residues 17 to 696 and 17 to 694 from a total of 702 and 700 of Cibeles and Demetra, respectively, in all subunits. Both proteins are structurally very similar [root mean square deviation (RMSD) of Cα positions between 678 aligned residues is 0.41 Å, below 0.5 Å as a standard cutoff of negligible differences] and contain a high percentage of aromatic residues (Y + F + W content of 19.3% in Cibeles and 18.9% in Demetra). Therefore, they can be classified as a particular type of aromatic-rich hexamerins called arylphorins. Close inspection of the atomic model revealed a complex interaction network between subunits in a trimer but, more importantly, each subunit of one trimer makes extensive contacts with a monomer of the opposing ring, related by a twofold axis [surface area between chains A/D 2258 $Å^2$, B/E 2264 $Å^2$, C/F 2269 $Å^2$, and −30 kcal/mol free energy for each dimer (*37*)], which is consistent with a stable interaction. Therefore, the hexamer can be described as a trimer of Cibeles-Demetra dimers (Fig. 3B), an arrangement that has also been reported for other arylphorins (*38*, *39*).

To further confirm these results, we separated the saliva protein content by SDS–polyacrylamide gel electrophoresis (PAGE) and extracted the proteins from the corresponding bands, which were subjected to N-terminal sequencing. The analysis confirmed that both proteins were present in *G. mellonella*'s saliva and that they started at amino acid number 17 (Cibeles, $_{17}$GYPQY$_{21}$; Demetra, $_{17}$GYPLFNN$_{23}$), indicating that the characteristic secretion signal peptide commonly present in this type of proteins had been proteolyzed (Fig. 2A). This event is expected in proteins found in a secretion medium, such as the ww saliva. These results, thus, validated our structural observations and corroborated that the reconstruction corresponds to secreted mature proteins.

The EM density also revealed clear sugar moieties present in both proteins (Fig. 3, B and C). In particular, each monomer is glycosylated at two sites, one located in the cleft formed at the Cibeles-Demetra interface (Asn$^{211}$ in both proteins) and the other found in the external face of the monomer (Asn$^{481}$ in Cibeles and Asn$^{479}$ in Demetra), branching out from the Ig-like subdomain and making contact in cis with the N-terminal region of the same monomer (Fig 3, B and C). The presence of glycosylations has been described in other arylphorins, in which they are frequently involved in protein folding and stabilization (*38*–*40*).

Notably, although the 3D classification showed that the main fraction (>50%) of Demetra and Cibeles molecules assemble into a stoichiometric complex, the rest of the particles separated into groups that apparently contained different protein ratios (fig. S1). In these more variable groups, one ring is always formed by three

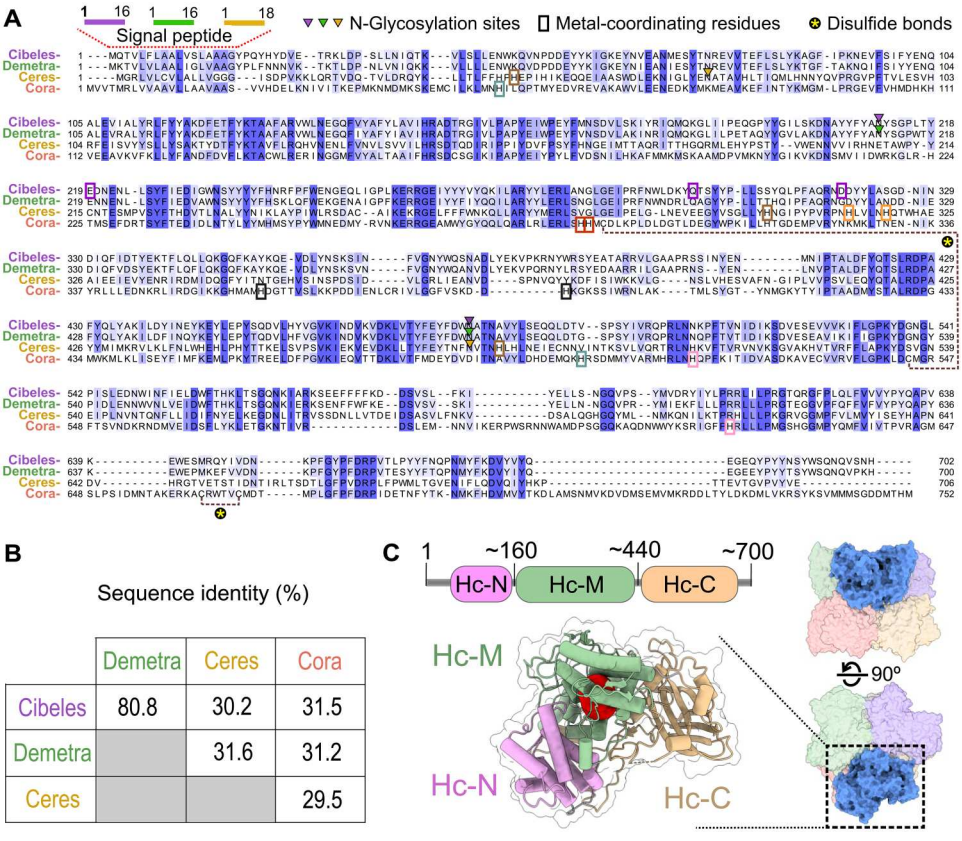


**Fig. 2. Sequence alignment and overall architecture of the four proteins present in *G. mellonella* saliva.** (**A**) Amino acid sequence alignment colored by similarity. Principal metal-coordinating residues are highlighted with squares, glycosylated residues are marked with triangles, and disulfide bridges are indicated with asterisk. (**B**) Pairwise sequence identity percentage between the four factors. (**C**) Overall primary, tertiary, and quaternary structure of the hemocyanin/phenoloxidase (Hc/PO) family members (*Panulirus interruptus* Hc, PDB code 1HCY, is used as example). Canonical copper-binding site is highlighted with red spheres.

molecules of Cibeles, but the density of the subunits of the second ring did not allow unambiguous identification.

To further characterize the sample, we purified the ww saliva with two consecutive ion exchange columns in which the peaks separated in the first run were re-loaded again so that a homogeneous sample was obtained for crystallization. Different crystal types grew, which showed x-ray diffraction of variable quality. Given that we did not know the content of the crystals, the structure of the best diffracting crystals was solved by molecular replacement (MR) by using all different cryo-EM structures as searching models. The heterohexamer Demetra-Cibeles yielded the highest molecular replacement score in all cases. However, after model refinement, the crystal structures revealed the presence of a homohexamer of Cibeles, supporting the idea that this protein can form different oligomeric assemblies (Fig. 3D and table S2). Before data collection, a metal scan by x-ray fluorescence spectroscopy indicated the presence of copper; thus, data were collected at the Cu absorption edge. The corresponding anomalous difference maps showed six clear peaks, one per monomer at the interface between the two rings of Cibeles. Thus, a Cu was in an octahedral coordination sphere that includes four oxygens on the plane and two in apical positions, from $Glu^{219}$ and $Asp^{318}$ carboxylates, $Gln^{299}$ main-chain carbonyl, and from water molecules bound to by $Asp^{220}$ and $Asp^{319}$, all from the same monomer, and facing the same arrangement in a second subunit at an 11-Å distance (fig. S3A). The cryo-EM reconstruction of the 3:3 heterocomplex showed a similar density in the three monomers of Cibeles. However, the density in the equivalent position in Demetra appeared smaller, likely due to the $Asp^{318}$ to $Gly^{318}$ substitution, and it was therefore modeled as a water molecule for this protein (fig. S3B).

Overall, these results show that Demetra associates with the highly related arylphorin Cibeles in *G. mellonella* saliva mainly to form trimer of heterodimers, although other stoichiometries (including Cibeles homohexamers) can also be found. Both factors contain glycosylations, commonly found in this type of proteins, and a metal ion can be localized (at least in each Cibeles monomer) in a position unrelated to the Hc/PO site. When recombinant Cibeles homohexamers were applied on a PE film, no modification could be detected (as indicated by RAMAN analysis; fig. S4A), confirming previous results (*21*).

## Ceres is a metal-binding hexamerin

After image processing, a small subgroup of particles (18,461) converged into a 2.8 Å reconstruction that clearly corresponded to a homohexamer of Ceres (Fig. 1 and fig. S1), a protein that has been previously identified in saliva and that has been shown to have a PE-degrading activity (*21*). Ceres also belongs to the hexamerin family and shares the same overall fold and quaternary structure as Demetra and Cibeles (Cα RMSD between 622 aligned

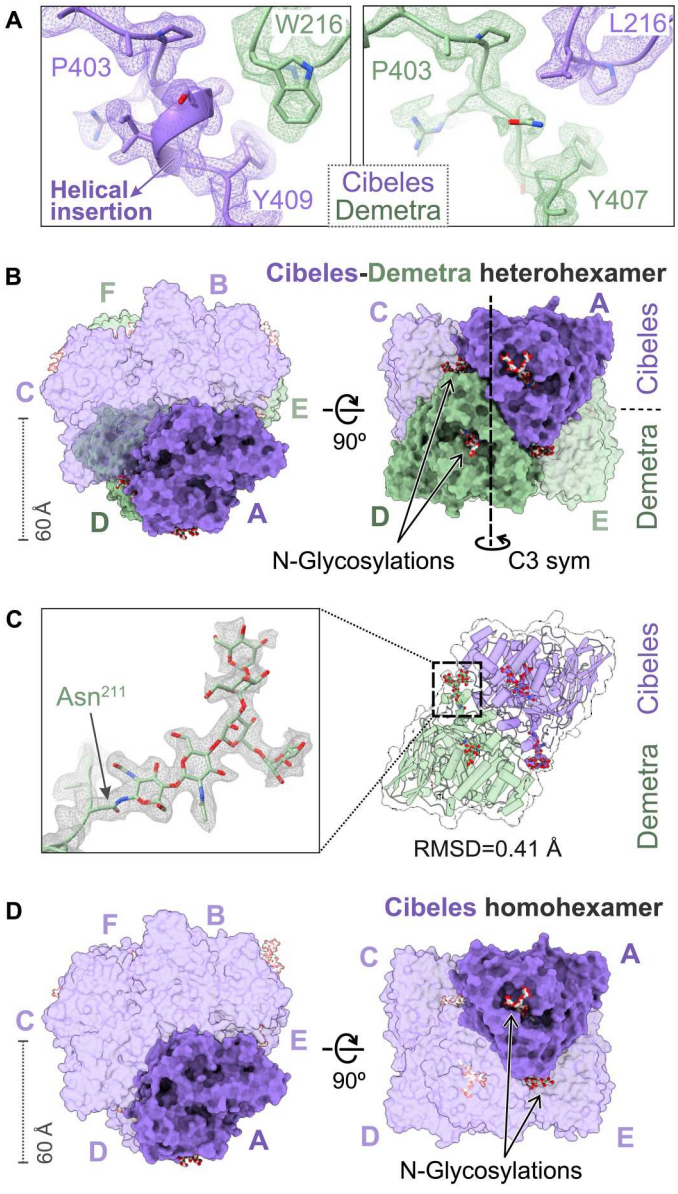


**Fig. 3. Three-dimensional structures of the arylphorins Demetra and Cibeles.** (**A**) Details of equivalent areas of different monomers in the reconstruction that show that the quality of the electron microscopy (EM) map allowed to differentiate and build the structures of Demetra and Cibeles. (**B**) Two orthogonal views of the 3:3 trimer of dimers formed by Demetra and Cibeles. Proteins are shown as surface representation and glycosylations as sticks. One monomer of each trimer is highlighted as solid surface. (**C**) Detailed view of a Demetra-Cibeles dimer (right). Inset: Close-up region showing the EM density and model of an oligosaccharide. (**D**) Crystal structure of the Cibeles homohexamer.

residues of 2.76 and 3.0 Å, respectively), although in this case the protein exclusively self-assembles into homohexamers (Fig. 4A).

The quality of the reconstruction allowed us to model residues 31 to 695 from this 706–amino acid–long protein. Although the limited amount of sample in SDS-PAGE prevented us from performing N-terminal sequencing, a previous report also indicated the presence of a signal peptide that is processed during the maturation process of this factor (*41*). The density, moreover, revealed the presence of two glycosylations, one located close to the threefold symmetry axis of the structure ($Asn^{73}$) and the other at the C-terminal subdomain ($Asn^{477}$) (Fig. 4A).

In addition, in the EM map, strong electron density peaks suggested that several metal ions, at least two per monomer, were present close to histidine residues. Since metal-bound hexamerins show the presence of copper at reaction centers rich in histidines, we modeled them as $Cu^{2+}$, although we cannot completely rule out that they might correspond to other atoms with similar coordination geometry (Fig. 4B). One of these ions is coordinated by two histidines ($His^{314}$ and $His^{319}$), each one contributed from a different monomer (fig. S5A). A second metal ion is coordinated by a cluster of histidines close to the dimerization interface (Fig. 4B, right panel). This cluster is close to the surface of the protein and located near the interface between trimeric rings, in sharp contrast with the internal position of the di-copper binding site characteristic of Hcs and POs (Figs. 2C and 4B). The His residues that typically form the oxygen-binding pocket at the core of Hcs/POs are not conserved in Ceres (same as in Demetra and Cibeles). Close to that position there is a cavity that contains an elongated density (Fig. 4C). However, the flexibility and/or partial occupancy of this ligand did not allow unambiguous identification.

Altogether, these results reveal that Ceres is a glycosylated metal-binding hexamerin that seems to engage organic molecules and that self-assembles into homohexamers. This protein, which appears to bind a yet unidentified organic ligand in a cavity close to the position of the canonical Hc/PO site, contains at least two metal ions within each monomer in remarkably different positions compared to the ones described in Cibeles, Hcs and POs.

## Cora, a methionine-rich hexamerin, is the most abundant protein in *G. mellonella*'s saliva

The largest group of particles (258,795 in the final reconstruction) yielded an excellent EM reconstruction (Fig. 1 and fig. S1), with a Fourier shell correlation that extended beyond the physical resolution limit (fig. S2, A and B). The 1.9-Å map, obtained using the superresolution images, allowed us to trace the polypeptide and unambiguously identify this factor as a methionine-rich hexamerin that we have termed Cora (bJHSP1; XP_026749149) (Fig. 5A). This result corroborates the finding in previous MS analysis that showed the presence of this factor in the ww saliva (*21*). We could model residues 34 to 739 (of the total 752 amino acids) into the EM density, revealing that the protein, which is characterized by a high content in sulfur-containing amino acids (8.9% Met), oligomerizes into a homohexamer that shares the overall fold and quaternary organization of the previously described factors (Fig. 5A).

Analysis of the monomer revealed the presence of two intramolecular disulfide bonds (C293-C544 and C663-C668), which could give this protein an increased stability and may in part explain the high resolution of the data (Fig. 5B). In agreement with most methionine-rich hexamerins, and in contrast with the other hexamerins present in the saliva, Cora does not contain any glycosylation. Strikingly, however, the C-terminal region of the protein folds back into the cleft formed between the two rings and appears to mimic the position of some of the glycans found in other members of this family of proteins (Fig. 5C).

The EM reconstruction showed four peaks of density, coordinated in all cases by two histidines, which likely correspond to

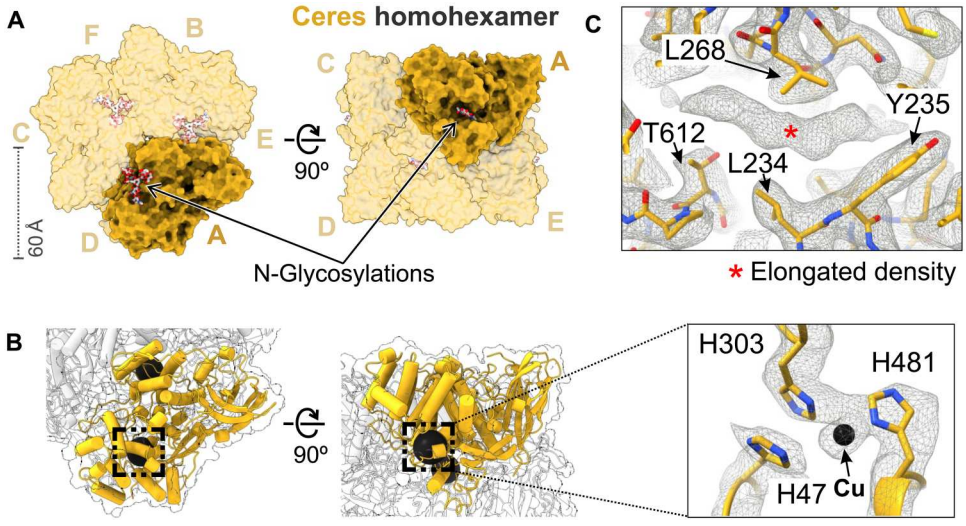


**Fig. 4. Cryo–electron microscopy (cryo-EM) reconstruction of Ceres.** (**A**) Overall organization of the homohexamer. Protein depicted as surface and glycosylations as sticks. One of the six monomers is highlighted as solid surface. (**B**) Two views of a Ceres monomer. Metal ions shown as black spheres. Inset: Close-up view of the coordination of one of the metal ions. (**C**) Depiction of the elongated density (visualized at a threshold value of 0.020) found at the core of Ceres monomers and some of the surrounding residues.

coordinated metal ions. As in the case of Ceres, we modeled them as $Cu^{2+}$ due to the coordination geometry and presence of this particular metal in other members of the superfamily (Fig. 5D, left panels, and fig. S5B). The copper ions are not clustered in the Hc/PO site that, similarly to all hexamerins, is not conserved in this factor either. The metals can be found evenly distributed around the monomeric structure separated by long distances (ranging from ~20 to 50 Å), a feature that, to the best of our knowledge, has not been described for this type of proteins (Fig. 5D, left panels, and fig. S5B). A free tryptophan can be seen in a pocket stabilized by multiple interactions (Fig. 5D, right panels). The role of this amino acid is yet unclear. However, stably associated free tryptophan residues have been described to play allosteric or structural roles in other proteins (*42*, *43*).

Together, the image analysis of the largest group of cryo-EM particles revealed that one of the principal proteins present in the ww saliva is Cora. This factor, as opposed to the previously described proteins, is an un-glycosylated, methionine-rich hexamerin capable of binding free tryptophan. Furthermore, among the four identified hexamerins, Cora shows an unusual abundance of metal ions, strikingly all in a position unrelated with the classic PO catalytic site.

### Cora degrades PE

Demetra and Ceres have been previously shown to degrade PE to different degrees (*21*). To test whether Cora had the capacity to oxidize PE, drops of 5 μl of purified recombinant protein (concentration, 1 to 2 μg/μl) were applied 8 to 10 consecutive times to a commercial PE film. Confocal Raman microscopy/Raman spectroscopy (RAMAN) analysis indicated oxidation of the PE polymer (Fig. 6, A and B), which was clearly evident when compared with control PE, showing the classical PE signature (Fig. 6, C and D). Inactivated Cora did not cause any modification on the PE film (fig. S4B).

Further, we analyzed the degradation by-products by gas chromatography–mass spectrometry (GC-MS). After 24 applications of 10 μl (concentration, 1 to 2 μg/μl), of 90 min each, compounds appeared in the experimental sample consisting of 2-ketons of 10 to 22 carbons (Fig. 6E). A longer PE treatment with Cora, from 6 to 12 applications, generated a rise in the relative amount of the 2-ketons of 14 to 18 carbons, and the appearance of 2-dodecanone, which was not present after 6 applications (Fig. 6F). Thus, the GC-MS outcome revealed that more compounds appeared with longer exposure of PE to Cora.

Overall, these data showed the effectiveness of Cora in degrading PE, which, together with the already described Demetra and Ceres (*21*), is the third enzyme contained in the ww saliva with the capacity of oxidizing plastic.

## DISCUSSION

The findings presented here shed light on the composition and molecular organization of the main proteins found in *G. mellonella*'s saliva. Cryo-EM analyses of the native sample provided valuable information that would be difficult to obtain from recombinant proteins. The 3D reconstructions revealed that the buccal secretion contains a mixture of four highly related proteins with very different proportions and distinct structural features [see (*21*) and Fig. 1]. Of these factors, recombinant Demetra, Ceres, and Cora showed the ability to degrade PE.

The ability of the ww hexamerins to oxidize PE evidences their potential interest in the development of biotechnological applications and paves the way to new approaches to plastic degradation by biological means. The biodegradation of polyolefin such as PE, PS, and PP is hindered to date by the inability of microorganisms to effectively oxidize plastics, a crucial step in the subsequent microbial bioassimilation (*5*). The proteins in the ww saliva might be used in combination with classical biodegradation protocols to achieve the biological conversion of plastics to $CO_2$ and $H_2O$ (*5*, *7*, *25*). The

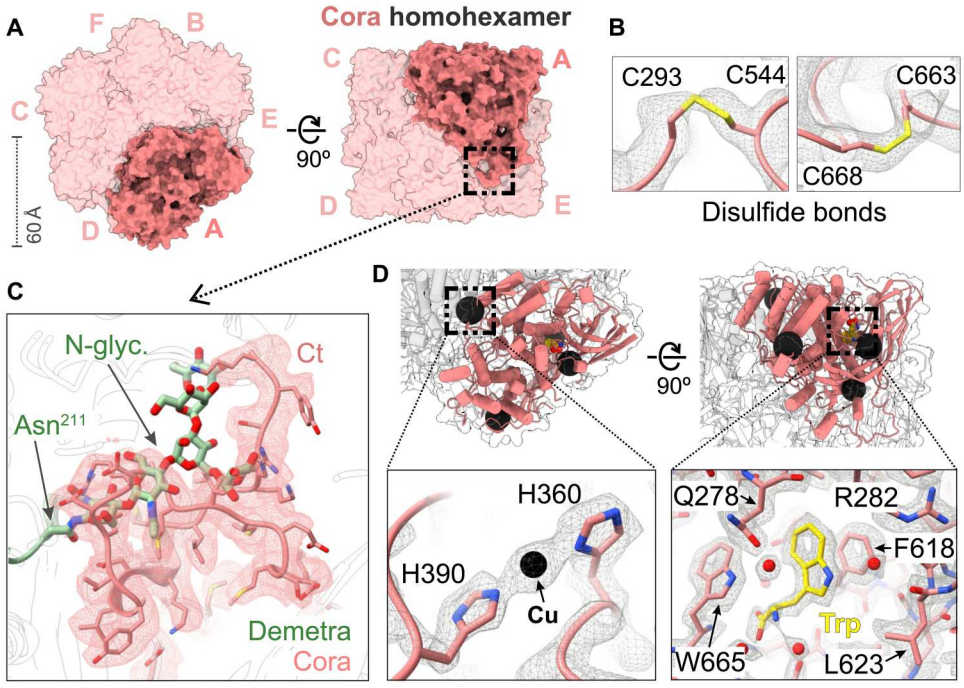


**Fig. 5. Three-dimensional architecture and analysis of Cora.** (**A**) Two orthogonal views of the homocomplex. One of the six monomers is highlighted as solid surface. (**B**) Detailed views of the two disulfide bridges present in the protein contoured at a threshold value of 0.013. (**C**) The C-terminal region of Cora occupies the same position of some of the oligosaccharides present in the other hexamerins described in this work. (**D**) Cartoon representation of a monomer of the protein showing the localization of the metals (black spheres) and the free tryptophan (yellow sticks). Insets: Detailed views of the interaction with one of the metal atoms (left) and the free tryptophan (right).

aggressive abiotic pretreatments currently used to oxidize the polymer (*5*, *7*) could be substituted by enzymatic activities operating in the same environment as the bioassimilating microorganisms, thus simplifying the logistic complexity of the process. Alternatively, the ww proteins could be used in a purely enzymatic setting together with other potential factors capable of modifying the degradation products resulting from PE oxidation, like the ketones described here [and elsewhere (*21*)]. Transformation of ketones in esters (or their carbonates) can be achieved using, for instance, biocatalysts, being an active field of research for potential biotechnology applications [reviewed in (*44*)]. Another possibility envisions the deployment of the resulting short oxidized molecules within an upcycling strategy framework. Aliphatic methyl ketones are valuable compounds in the chemical industry, as revealed by efforts in producing them via fermentation using engineered bacteria (*45*–*47*).

The proteins in the saliva of ww belong to the hexamerin family, a group of proteins widespread in insects. The extraordinary diversity found within this family of proteins (*48*) has translated into a highly heterogeneous nomenclature. Thus, while some hexamerins were named juvenile hormone suppressible proteins owing to their apparent regulation by this hormone (*49*), other hexamerin members were termed according to their particular amino acid content (*50*) or their ability to bind certain vitamins (*51*). Despite the dispersed terminology, phylogenetic analyses have demonstrated that all hexamerins are actually orthologous proteins (*48*). To date, some of these proteins are assumed to act as storage proteins, with a supposed role in the insect ontogeny (*52*). However, the exact function of most hexamerin members is unclear.

Hexamerins are phylogenetically related to Hcs and POs (*32*). Hcs and POs are classified, together with tyrosinases and catechol oxidases, as type 3 copper proteins, a protein family characterized by the presence of two copper atoms each coordinated by three histidines (*53*). Although the Cu active site location is highly conserved among type 3 copper proteins, they exhibit a wide range of activities and are involved in a variety of biological processes (*53*, *54*). For instance, despite sharing a common active site, only POs have been cataloged as enzymes, capable of oxidizing phenols and involved in cuticle sclerotization and melanization as an immune response against invading microorganisms (*55*). In contrast, Hcs have traditionally been considered oxygen transport proteins devoid of any catalytic function. However, a Hc from a wood-boring crustacean has been recently reported to be able to degrade lignin, while other studies have revealed a hidden enzymatic activity in other Hc members using different conditions and activation mechanisms (*56*–*61*), highlighting the rich enzymatic potential of these proteins (*56*–*61*).

Despite being relatively close homologs, hexamerins lost the ability to bind copper in the Hc/PO canonical active site at some point in evolution. In agreement with this observation, the residues involved in $Cu^{2+}$ coordination in Hcs and POs are not conserved in any of the four main proteins present in the ww saliva (Fig. 7). Instead of the conserved histidine residues found in POs and Hcs, the cavity is mainly lined with a combination of aromatic/hydrophobic and charged residues (Fig. 7). The reconstructions revealed the presence of abundant metal atoms in other markedly different positions (Fig. 8A and fig. S6). The diverse location of metal sites, sometimes present at interfaces between subunits, might point to a

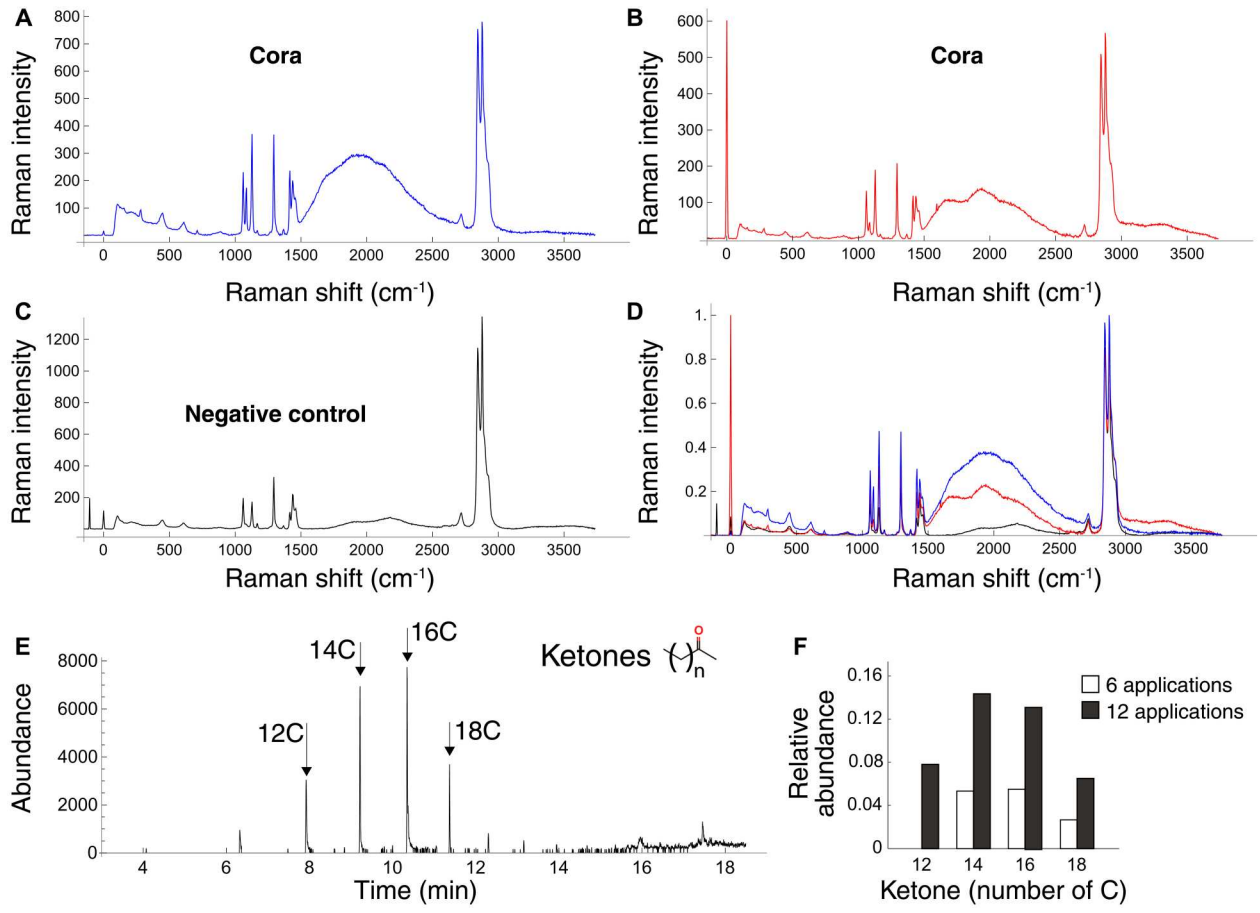


**Fig. 6. RAMAN analysis and identification via gas chromatography–mass spectrometry (GC-MS) of the degradation by-products of polyethylene (PE) film treated with purified recombinant Cora.** (**A** and **B**) PE film treated with Cora. The peaks between 1500 and 2400 $cm^{-1}$ indicate PE deterioration. Oxidation is indicated between 1600 and 1800 $cm^{-1}$ (carbonyl group) and 3000 and 3500 $cm^{-1}$ (hydroxyl group) [evident in (B)]. (**C**) Control PE film. PE signature is characterized by the peaks at 1061, 1128, 1294, 1440, 2846, and 2880 $cm^{-1}$. (**D**) Overlapping normalized profiles (A to C). (**E**) Chromatogram of the fragmentgram of the ion mass/charge ratio (*m*/*z*) 58 from methyl ketones of PE treated with the enzyme. The arrows indicated the peaks corresponding to 2-ketones with different numbers of carbons. (**F**) Variation of PE degradation by-products via GC-MS after different increases of ketone formation as degradation products from 6 to 12 applications of Cora to PE, with an increase of 2-ketones formation by doubling applications of the enzyme to PE.

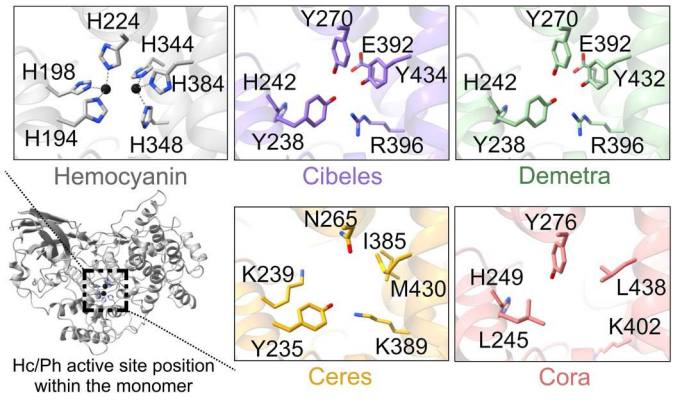


**Fig. 7. Comparison between the metal-binding site of hemocyanins (Hcs) and the equivalent residues of the hexamerins present in *G. mellonella*.** Canonical di-copper binding center in *P. interruptus* Hc (PDB code 1HCY) and the corresponding sites of the hexamerins present in wax worm (ww) buccal secretion.

structural or allosteric function, although it cannot be excluded that the PE-modifying activity of these proteins is assisted by any of these metals. The fact that metals are also present in Cibeles, the hexamerin without any apparent effect on PE, adds to the conundrum. Thus, whether this activity lies in the Hc/PO internal pocket or can be found in a more solvent-exposed position, as has been described for other plastic and lignin-degrading enzymes (*31*, *62*–*64*), is an intriguing question. This issue is further complicated by the fact that the sequence and structural similarities among the four hexamerins do not clearly reveal a shared canonical catalytic site (fig. S7).

Surface analysis of the proteins showed a variable distribution of charges [which on average agreed with their isoelectric point (pI) values] and the presence of different clefts and cavities that, in some cases, are occupied by glycosylations (Fig. 8B and fig. S6B). In addition, the high-resolution structures pointed out that no cofactors implicated in typical oxidation processes (such as nicotinamide or flavin derivatives) are present in the analyzed ww proteins, in agreement with the absence of these types of molecules

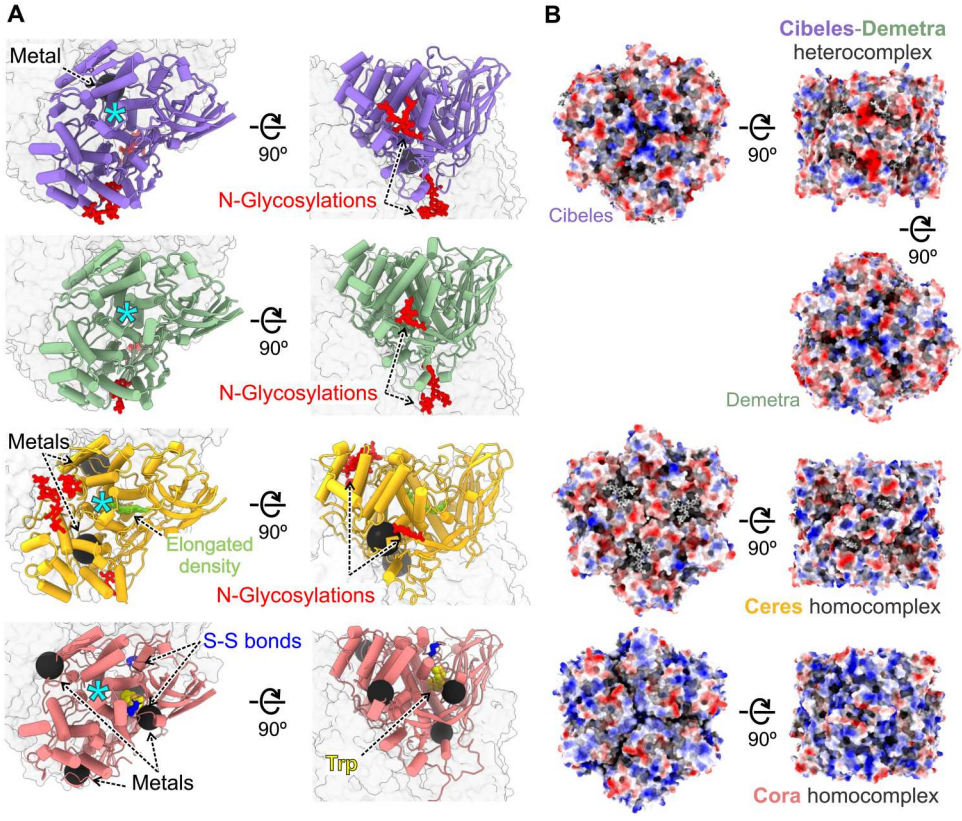


**Fig. 8. Structural comparison between the four hexamerins in wax worm (ww) buccal secretion.** (**A**) Two orthogonal views of Cibeles (purple), Demetra (green), Ceres (yellow), and Cora (red). The position of the classic di-copper hemocyanin/phenoloxidase (Hc/PO) binding center is indicated with a blue asterisk. (**B**) Electrostatic surface potential. The negatively and positively charged surfaces are colored in red and blue, respectively.

in the Hc/PO family. However, the structures of Ceres and Cora contain extra densities in similarly positioned binding pockets (Fig. 8A). Although the flexibility (and perhaps partial occupancy) did not allow unambiguous identification, the cryo-EM density shows that Ceres engages an elongated molecule in this position (Figs. 4C and 8A). The cryo-EM density in Cora, on the other hand, clearly corresponds to a free tryptophan (Fig. 5D, right panels, and 8A). Whether these molecules participate in PE modification or have a regulatory role needs to be established.

Our results show that elucidating at this point the precise mechanism of action of the ww hexamerins is far from trivial, due to their structural variability and heterogeneous posttranslational modifications, together with the lack of a known natural substrate. The difficulty to characterize the mechanisms underlying the enzymatic degradation of plastics is well illustrated by the case of PETases, enzymes that exhibit a highly efficient degradation activity toward PET (*26*–*30*). In contrast to the factors presented here, PETases belong to the cutinase/hydrolase family, a well-characterized group of monomeric proteins that act on their substrates through a highly conserved catalytic triad (*28*, *30*, *62*, *65*, *66*). Despite the relative homogeneity of these enzymes, it took years of collective efforts to shed light on their substrates and mechanism of action, highlighting the extent of complexity common to this type of studies.

Considering that these proteins did not evolve to degrade PE, understanding the role of these hexamerins in the life cycle of *G. mellonella* remains an outstanding question, fundamental also to addressing their ability to degrade PE. Why the ww produces four similar but different proteins, all of which find their way into the worm buccal cavity? A potential answer to this question emerges from the ability of hexamerins to bind small organic metabolites like riboflavin (*51*) or biliverdin (*67*) with high affinity. The capacity to interact with small molecules is also reflected in the reported binding to insecticides, which points to a role in detoxification of xenobiotics (*68*). In this regard, members of this family have been shown to neutralize the action of toxic phenolics (*69*), a chemical defense widely used by plants against herbivore insects. Although *G. mellonella* larvae are not directly herbivores, they live inside beehives, where they are exposed to a wide range of compounds of plant origin, such as pollen, propolis, and honey, all rich in phenolics. The necessity to interact with and neutralize phenolics could be related to their PE-degrading activity, as discussed elsewhere (*21*). However, future studies are required to confirm or discard this idea.

Overall, the PE-degrading activity described in this work and elsewhere (*21*) highlights the functional plasticity and biotechnological potential of the hexameric factors found in the ww saliva. The discovery of these factors widens the potential application of biological systems to manage plastic waste, beyond the current paradigm of biodegradation by microorganisms. This path is not free of challenges, both at the basic research level (for example, potential degradation of mixed plastics or blends) and at the industrial level (scaling up of protein production, optimization of reaction

efficiency, etc.) The detailed structural characterization described here is a necessary step toward the development of this emerging field. The combined analyses of x-ray crystallography and cryo-EM reveal a rich and complex landscape within a group of invertebrate proteins, which has received very limited attention in life sciences. The observed heterogeneity of this type of proteins suggests a convoluted relationship between structure and function. Future studies will contribute to unveiling the molecular basis underlying the activity of these proteins, together with their role in the biology of *G. mellonella* larvae, opening new venues for plastic degradation based on highly efficient natural means.

## METHODS

### Sample preparation for structural analysis and N-terminal sequencing

Saliva from *G. mellonella* larvae was extracted using a glass capillary connected to a mouth pipette. The sample was mixed 1:1 with a buffer containing 50 mM tris-HCl (pH 8), 100 mM NaCl, and 2 mM DL-dithiothreitol (DTT), aliquoted, and flash-frozen in liquid nitrogen. For N-terminal sequencing, the sample was run on an SDS-PAGE gel and the bands were transferred to a polyvinylidene difluoride (PVDF) membrane (Bio-Rad). N-terminal Edman degradation was carried out using the Procise 494 HT Sequencing System (Applied Biosystems, Foster City, CA, USA) according to the manufacturer's instructions.

### Single-particle cryo-EM

For the EM experiments, *G. mellonella* saliva was serially diluted 250 times in 20 mM Hepes (pH 7.5), 50 mM NaCl, 0.5% glycerol, and 0.015% NP-40. Three microliters of the sample was applied to glow-discharged Quantifoil R 2/1 300 mesh grids (Quantifoil, Germany), covered with a homemade continuous carbon film, incubated during 1 min, blotted for 2 s (blot force 0), and frozen in liquid ethane using a Vitrobot Mark IV plunging system (Thermo Fisher Scientific).

Cryo-EM grids were first prescreened in a JEOL 1230 microscope equipped with a TemCam-F416 (TVIPS, Gauting, Germany) camera. High-resolution cryo–electron micrographs were recorded at a nominal magnification of 81,000x on a Titan Krios electron microscope (Thermo Fisher Scientific) operated at 300 kV using a Gatan BioQuantum K3 direct electron detector (LISCB, Leicester University). The images were collected in super-resolution counting mode using EPU (Thermo Fisher Scientific) at a calibrated pixel size of 1.086 Å/pixel (0.543 Å/pixel superresolution). The total dose was 58.3 electrons/Å$^2$ equally fractionated in 60 frames.

The collected movies were imported into Relion-3.1 (*70*) for data processing, where they were motion-corrected using motioncor2 (*71*). The contrast transfer functions (CTFs) were estimated using gctf (*72*). A total of 6089 micrographs were selected, after eliminating images with poor CTF estimation and ice contamination, and picked using templates that were generated using a small subset of the images. Following 2D classification, a total of 1,309,500 particles were selected from the initial ~1.82 million and extracted at 1.086 Å/pixel. These particles were subjected to a first round of 3D classification followed by 3D refinement, using D3 symmetry, which showed that the particles could be initially divided into two main groups. The largest group corresponded to Cora. 3D refinement of this population showed that the resolution was limited by the physical pixel size of the images and, therefore, the particles were re-extracted from the superresolution movies at 0.8 Å/pixel, which allowed us to obtain a 1.9 Å resolution structure of this factor. Close inspection of the second group particles indicated the presence of heterogeneity. These particles were subjected to a second and third rounds of 3D classification and refinement that revealed that this population was composed of a small subgroup that corresponded to Ceres (2.8 Å) and a larger one that clearly corresponded to the arylphorins. Although the high sequence similarity (81%) did not initially allow to differentiate Demetra from Cibeles, performing a 3D classification run with local searches and symmetry relaxation allowed us to determine that this group of particles was formed by Demetra-Cibeles heterocomplexes mainly in a 3:3 ratio (>50% of the particles) (note that, since the official distribution only supports symmetry relaxation for cyclic symmetries, this step was carried out with the Relion-3.1 version compiled by S. Ilca; https://github.com/serbanilca/relion-3.1-relax). The particles from the Demetra-Cibeles trimer of dimers were further refined with C3 symmetry to produce a 2.3 Å map.

Homology models of the proteins were generated using SWISS-MODEL server (*73*) and used as starting points to manually build the individual monomers in COOT (*74*). The monomers were then subjected to iterative rounds of model building and real-space refinement with COOT and PHENIX (*75*) using Ramachandran, rotamer, geometry, and secondary structure restraints. The complete models were generated applying D3 (to Ceres and Cora monomers) and C3 (to the Demetra-Cibeles heterodimer) symmetry operators to the asymmetric units. The final model was achieved by consecutive rounds of real-space refinement performed with PHENIX applying non-crystallographic symmetry (NCS) constraints. The quality of the model was assessed with MolProbity from Phenix package, the validation tool from PDB (OneDep), and different validation tools from COOT. All structure figures were generated with ChimeraX 1.4 (*76*).

### Protein crystallization and x-ray data collection

Aliquots of 120 µl of saliva extracted from several ww individuals were diluted in buffer A [10 mM tris-Cl (pH 8) and 50 mM NaCl], flash-frozen in liquid nitrogen, and stored at −80°C. For crystallization trials and optimization, one aliquot was thawed on ice, centrifuged for 10 min at 16,000 rpm, filtered with 0.45-µm pore filters, loaded to an Q FF anion exchange chromatography column (Thermo Fisher Scientific) equilibrated with buffer A, and washed until recovery of the buffer baseline. It followed a gradient with buffer B [10 mM tris-Cl (pH 8) and 500 mM NaCl], and eluting fractions were analyzed by 12% SDS-PAGE. All fractions showing proteins of hexamerin size were pooled, the NaCl concentration estimated to subsequently dilute the salt concentration to 25 mM (totaling 200 ml), and loaded to a monoQ 5/50 GL ion exchange column (Cytiva) equilibrated with buffer A. After a wash step, a gradient with buffer B was applied. The different hexamerins had very similar molecular mass but they eluted in different yet not completely well-resolved peaks from the monoQ. To detect heterogeneity that would impair crystallization, the protein concentration was estimated for each fraction and equal amounts of sample were loaded in a 10% SDS-PAGE run at 50 V. Only those fractions corresponding to the same chromatographic peak and showing a single band in SDS-PAGE were pooled, diluted to reach 25 mM NaCl and

reloaded to the monoQ. The eluted fractions from every chromatographic peak and single band in SDS-PAGE were pooled, concentrated to 1 mg/ml, and set for crystallization screenings with sitting-drop 96-well plates (Molecular Dimensions) at the Automated Crystallization Platform at the Barcelona Science Park. The successful crystallization conditions were manually optimized with 24-well plates. Cibeles homohexamer crystallized in 35% 2-methyl-2,4-pentanediol (MPD), 100 mM $Li_2SO_4$, and 100 mM MES (pH 6). Crystals were cryoprotected with 20% glycerol added to the crystallization solution and flash-frozen in liquid nitrogen.

Crystals (of unknown content) were tested at ID30B beamline from the European Synchrotron Radiation Facility (ESRF; Grenoble, France). Crystals were systematically scanned for metals in the range from 6 to 20 keV, which covers most of the elements naturally present in macromolecules. X-ray diffraction data were collected from different crystal regions and at the corresponding metal absorption edge . Data were processed, scaled, and merged with XDS and XSCALE (*77*) with unmerged Friedel pairs. Molecular replacement (MR) was followed by PHASER (*78*) using all cryo-EM structures as searching models. Demetra/Cibeles cryo-EM heterohexamer systematically rendered the highest score in all cases [Translation function Z-score (TFZ) 97.1 versus 14 to 17 with the other cryo-EM structures], so the crystal with the highest resolution (2.2 Å) collected slightly above the Cu absorption edge (9.2 keV) was used for automated model building with PHENIX (*75*) in $P2_12_12_1$ as determined by MR. Visual inspection of the structure and real-space refinement was done with COOT (*74*), which alternated with automatic refinement of atomic positions with PHENIX (*74*). The atomic refinement clearly indicated the presence of a Cibeles homohexamer. Stereochemistry validation was done with the Protein Data Bank validation service. The metal scan rendered a fluorescence peak at 8.03 keV, consistent with $Cu^{2+}$ emission. Calculation of an anomalous map resulted in a clear peak consistent with a metal coordinated by aspartic and glutamic carboxylates and a carbonyl, at a distance of 2.3 Å slightly large for Cu coordination.

### Cora recombinant protein production and utilization

Basic Juvenile Hormone Suppressor 1 (bJHSP1) (termed Cora) was produced by GenScript, using the baculovirus expression system in insect cells, according to the manufacturer. Briefly, Sf9 cells were infected with P2 baculovirus, flasks were incubated at 27°C for 48 to 72 hours, and media were harvested. Then, cells were removed, and transfection medium was applied for purification. The produced proteins were resuspended in 50 mM tris-Cl, 500 mM NaCl, 10% glycerol, 0.5% sodium lauroyl sarcosine, 2 mM tris(2-carboxyethyl)phosphine (TCEP), and 2 mM glutathione (pH 7.5). The degradation assay was as previously described (*21*). The same buffer alone was used as negative control.

### RAMAN analysis

PE film was treated with recombinant protein as follows: 5 µl of protein (concentration between 1 and 5 µg/ml) was applied eight times on PE film 90 min each time. For the control with inactivated protein, recombinant protein was denatured at 100°C for 10 min. Treated and control films were washed with water and ethanol. RAMAN analyses were performed on (treated and control) PE films using Alpha300R − Alpha300A AFM Witec equipment with 5 mW power, 50× (numerical aperture 0.8) objective, integration time 1, accumulation 30, and wavelength 532 nm.

### Gas chromatography–mass spectrometry

Following procedures previously described in (*21*), an amount of 20 mg of PE 4000 was placed in a 1.5-ml Eppendorf tube. PE was exposed to 10 µl (1.5 mg/ml) of recombinant Cora, 24 times for 90 min. Prolonged treatment was also performed for Cora (days 1 and 2), six applications per day of 10 µl (1.5 mg/ml) for 90 min each. As control, the same experiment was repeated using the protein buffer. Afterward, samples were centrifuged with an Eppendorf centrifuge 5810 R at 19,083*g* for 30 s and the supernatant was transferred to a new 1.5-ml Eppendorf tube. Samples and controls were extracted using a QuEChERS (quick, easy, cheap, effective, and safe) method (*79*) based on the conditions used in a previous work (*80*) with some modifications. Briefly, 50 µl of diphenyl phthalate [internal standard (IS)] at a concentration of 1 mg/ml was added to each sample and extracted with 300 µl of dichloromethane (DCM) and 5% [volume/mass (v/m)] of NaCl. The tube was vortexed for 30 s and sonicated in a bath (50/60 Hz) for 15 min at room temperature, followed by centrifugation with an Eppendorf centrifuge 5810 R at 20°C and 19,083*g* for 10 min. Finally, DCM located as the supernatant was collected and placed in an insert before analysis (*21*).

DCM (CAS no.: 75-09-2) for GC-MS was SupraSolv grade purity and obtained from Sigma-Aldrich (Darmstadt, Germany). Sodium chloride (NaCl; ≥99.5%; CAS no.: 7647-14-5) and ultrapure water from a Milli-Q system were supplied by Merck (Darmstadt, Germany). Crystalline granular powder PE (PE 4000; CAS no.: 9002-88-4, specification sheet in https://www.sigmaaldrich.com/ES/es/product/aldrich/427772) was supplied by Sigma-Aldrich (Saint Louis, USA) (*21*).

Chromatographic analyses were performed with GC-MS 7980A-5975C from Agilent Technologies. Separation of the metabolites was performed on the DB-5$^{th}$ Column coated with polyimide (30 m length, 0.25 mm inner diameter, and 0.1 µm film thickness; Agilent Technologies, USA) for proper separation of substances, and helium (He) was used as a carrier gas. The analysis was performed using a split injector at 350°C and an injection volume of 1 µl. The ion source temperature was 230°C, the °C mass spectral analysis was performed in scan mode, the quadrupole temperature was 150°C, and the fragmentation voltage was 70 eV. The oven program started at 60°C for 3 min, then 20°C/min to 350°C for 1 min. The total run time was 18.5 and 19.5 min for derivatized samples. The resulting chromatograms were processed using the software MSD ChemStation E.01.00.237 from Agilent Technologies Inc., while for the identification NIST11 library was used (*21*).

The evaluation of the prolonged treatment was based on the relative abundance of each untargeted compound, which consists of the quotient of the area under the peak of each compound divided by the area under the peak of the IS.

### Mass spectrometry

The protein identification by nano-scale liquid chromatographic–tandem mass spectrometry (nLC-MS/MS) was carried out in the Proteomics and Genomics Facility (CIB-CSIC), a member of ProteoRed-ISCIII network.

## Supplementary Materials

**This PDF file includes:**

Figs. S1 to S7
Tables S1 and S2

## REFERENCES AND NOTES


1. Plastics Europe; https://plasticseurope.org/.
2. J. M. Garcia, M. L. Robertson, The future of plastics recycling. *Science* **358**, 870–872 (2017).
3. R. Geyer, J. R. Jambeck, K. L. Law, Production, use, and fate of all plastics ever made. *Sci. Adv.* **3**, e1700782 (2017).
4. G. Suzuki, N. Uchida, L. H. Tuyen, K. Tanaka, H. Matsukami, T. Kunisue, S. Takahashi, P. H. Viet, H. Kuramochi, M. Osako, Mechanical recycling of plastic waste as a point source of microplastic pollution. *Environ. Pollut.* **303**, 119114 (2022).
5. A. C. Albertsson, The influence of biotic and abiotic environments on the degradation of polyethylene. *Prog. Polym. Sci.* **15**, 177–192 (1990).
6. M. Hakkrainen, A.-C. Albertsson, Environmental degradation of polyethylene. *Adv. Polym. Sci.* **169**, 177–200 (2004).
7. R. Wei, W. Zimmermann, Microbial enzymes for the recycling of recalcitrant petroleum-based plastics: How far are we? *J. Microbial Biotechnol.* **10**, 1308–1322 (2017).
8. N. Mohanan, Z. Montazer, P. K. Sharma, D. B. Levin, Microbial and enzymatic degradation of synthetic plastics. *Front. Microbiol.* **11**, 580709 (2020).
9. J. Yang, Y. Yang, W.-M. Wu, J. Zhao, L. Jiang, Evidence of polyethylene biodegradation by bacterial strains from the guts of plastic-eating waxworms. *Environ. Sci. Technol.* **48**, 13776–13784 (2014).
10. Y. Yang, J. Yang, W.-M. Wu, J. Zhao, Y. Song, L. Gao, R. Yang, L. Jiang, Biodegradation and mineralization of polystyrene by plastic-eating mealworms: Part 2. Role of gut microorganisms. *Environ. Sci. Technol.* **49**, 12087–12093 (2015).
11. Y. Yang, J. Yang, W.-M. Wu, J. Zhao, Y. Song, L. Gao, R. Yang, L. Jiang, Biodegradation and mineralization of polystyrene by plastic-eating mealworms: Part 1. Chemical and physical characterization and isotopic tests. *Environ. Sci. Technol.* **49**, 12080–12086 (2015).
12. P. Bombelli, C. J. Howe, F. Bertocchini, Polyethylene bio-degradation by caterpillars of the wax moth *Galleria mellonella*. *Curr. Biol.* **27**, R292–R293 (2017).
13. H. G. Kong, H.-H. Kim, J.-H. Chung, J. Jun, S. Lee, H.-M. Kim, S. Jeon, S. G. Park, J. Bhak, C.-M. Ryu, The *Galleria mellonella* hologenome supports microbiota-independent metabolism of long-chain hydrocarbon beeswax. *Cell Rep.* **26**, 2451–2464.e5 (2019).
14. A. M. Brandon, S.-H. Gao, R. Tian, D. Ning, S.-S. Yang, J. Zhou, W.-M. Wu, C. S. Criddle, Biodegradation of polyethylene and plastic mixtures in mealworms (Larvae of *Tenebrio molitor*) and effects on the gut microbiome. *Environ. Sci. Technol.* **52**, 6526–6533 (2018).
15. B. J. Cassone, H. C. Grove, O. Elebute, S. M. P. Villanueva, C. M. R. LeMoine, Role of the intestinal microbiome in low-density polyethylene degradation by caterpillar larvae of the greater wax moth, *Galleria mellonella*. *Proc. Biol. Sci.* **287**, 20200112 (2020).
16. Y. Lou, P. Ekaterina, S.-S. Yang, B. Lu, B. Liu, N. Ren, P. F.-X. Corvini, D. Xing, Biodegradation of polyethylene and polystyrene by greater wax moth larvae (*Galleria mellonella* L.) and the effect of co-diet supplementation on the core gut microbiome. *Environ. Sci. Technol.* **54**, 2821–2831 (2020).
17. Z. Montazer, M. B. Habibi Najafi, D. B. Levin, In vitro degradation of low-density polyethylene by new bacteria from larvae of the greater wax moth, *Galleriamellonella*. *Can. J. Microbiol.* **67**, 249–258 (2021).
18. A. Peydaei, H. Bagheri, L. Gurevich, N. de Jonge, J. L. Nielsen, Impact of polyethylene on salivary glands proteome in *Galleria melonella*. *Comp. Biochem. Physiol. Part D Genomics Proteomics* **34**, 100678 (2020).
19. J. Zhang, D. Gao, Q. Li, Y. Zhao, L. Li, H. Lin, Q. Bi, Y. Zhao, Biodegradation of polyethylene microplastic particles by the fungus *Aspergillus flavus* from the guts of wax moth *Galleria mellonella*. *Sci. Total Environ.* **704**, 135931 (2020).
20. Y. Yang, J. Wang, M. Xia, Biodegradation and mineralization of polystyrene by plastic-eating superworms *Zophobas atratus*. *Sci. Total Environ.* **708**, 135233 (2020).
21. A. Sanluis-Verdes, P. Colomer-Vidal, F. Rodriguez-Ventura, M. Bello-Villarino, M. Spinola-Amilibia, E. Ruiz-Lopez, R. Illanes-Vicioso, P. Castroviejo, R. Aiese Cigliano, M. Montoya, P. Falabella, C. Pesquera, L. Gonzalez-Legarreta, E. Arias-Palomo, M. Solà, T. Torroba, C. F. Arias, F. Bertocchini, Wax worm saliva and the enzymes therein are the key to polyethylene degradation by *Galleria mellonella*. *Nat. Commun.* **13**, 5568 (2022).
22. L. Ren, L. Men, Z. Zhang, F. Guan, J. Tian, B. Wang, J. Wang, Y. Zhang, W. Zhang, Biodegradation of polyethylene by *Enterobacter* sp. D1 from the guts of wax moth *Galleria mellonella*. *Int. J. Environ. Res. Public Health* **16**, 1941 (2019).
23. S.-S. Yang, M.-Q. Ding, Z.-R. Zhang, J. Ding, S.-W. Bai, G.-L. Cao, L. Zhao, J.-W. Pang, D.-F. Xing, N.-Q. Ren, W.-M. Wu, Confirmation of biodegradation of low-density polyethylene in dark- versus yellow- mealworms (larvae of *Tenebrio obscurus* versus *Tenebrio molitor*) via. gut microbe-independent depolymerization. *Sci. Total Environ.* **789**, 147915 (2021).
24. B. Serrano-Antón, F. Rodríguez-Ventura, P. Colomer-Vidal, R. A. Cigliano, C. F. Arias, F. Bertocchini, The virtual microbiome: A computational framework to evaluate microbiome analyses. *PLOS ONE* **18**, e0280391 (2023).
25. Z. Montazer, M. B. Habibi Najafi, D. B. Levin, Challenges with verifying microbial degradation of polyethylene. *Polymers (Basel)* **12**, 123 (2020).
26. R.-J. Müller, H. Schrader, J. Profe, K. Dresler, W.-D. Deckwer, Enzymatic degradation of poly(ethylene terephthalate): Rapid Hydrolyse using a Hydrolase from T. *fusca*. *Macromol. Rapid Commun.* **26**, 1400–1405 (2005).
27. S. Yoshida, K. Hiraga, T. Takehana, I. Taniguchi, H. Yamaji, Y. Maeda, K. Toyohara, K. Miyamoto, Y. Kimura, K. Oda, A bacterium that degrades and assimilates poly(ethylene terephthalate). *Science* **351**, 1196–1199 (2016).
28. V. Tournier, C. M. Topham, A. Gilles, B. David, C. Folgoas, E. Moya-Leclair, E. Kamionka, M.-L. Desrousseaux, H. Texier, S. Gavalda, M. Cot, E. Guémard, M. Dalibey, J. Nomme, G. Cioci, S. Barbe, M. Chateau, I. André, S. Duquesne, A. Marty, An engineered PET depolymerase to break down and recycle plastic bottles. *Nature* **580**, 216–219 (2020).
29. S. Kaabel, J. P. D. Therien, C. E. Deschênes, D. Duncan, T. Friščić, K. Auclair, Enzymatic depolymerization of highly crystalline polyethylene terephthalate enabled in moist-solid reaction mixtures. *Proc. Natl. Acad. Sci. U.S.A.* **118**, e2026452118 (2021).
30. C. Sonnendecker, J. Oeser, P. K. Richter, P. Hille, Z. Zhao, C. Fischer, H. Lippold, P. Blázquez-Sánchez, F. Engelberger, C. A. Ramírez-Sarmiento, T. Oeser, Y. Lihanova, R. Frank, H. G. Jahnke, S. Billig, B. Abel, N. Sträter, J. Matysik, W. Zimmermann, Low carbon footprint recycling of post-consumer PET plastic with a metagenomic polyester hydrolase. *ChemSusChem* **15**, e202101062 (2022).
31. S. Joo, I. J. Cho, H. Seo, H. F. Son, H.-Y. Sagong, T. J. Shin, S. Y. Choi, S. Y. Lee, K.-J. Kim, Structural insight into molecular mechanism of poly(ethylene terephthalate) degradation. *Nat. Commun.* **9**, 382 (2018).
32. T. Burmester, Origin and evolution of arthropod hemocyanins and related proteins. *J. Comp. Physiol. B* **172**, 95–107 (2002).
33. W. P. J. Gaykema, W. G. J. Hol, J. M. Vereijken, N. M. Soeter, H. J. Bak, J. J. Beintema, 3.2 Å structure of the copper-containing, oxygen-carrying protein *Panulirus interruptus* haemocyanin. *Nature* **309**, 23–29 (1984).
34. B. Linzen, N. M. Soeter, A. F. Riggs, H. J. Schneider, W. Schartau, M. D. Moore, E. Yokota, P. Q. Behrens, H. Nakashima, T. Takagi, T. Nemoto, J. M. Vereijken, H. J. Bak, J. J. Beintema, A. Volbeda, W. P. J. Gaykema, W. G. J. Hol, The structure of arthropod hemocyanins. *Science* **229**, 519–524 (1985).
35. S. L. Ilca, X. Sun, K. el Omari, A. Kotecha, F. de Haas, F. DiMaio, J. M. Grimes, D. I. Stuart, M. M. Poranen, J. T. Huiskonen, Multiple liquid crystalline geometries of highly compacted nucleic acid in a dsRNA virus. *Nature* **570**, 252–256 (2019).
36. V. Abrishami, S. L. Ilca, J. Gomez-Blanco, I. Rissanen, J. M. de la Rosa-Trevín, V. S. Reddy, J.-M. Carazo, J. T. Huiskonen, Localized reconstruction in Scipion expedites the analysis of symmetry mismatches in cryo-EM data. *Prog. Biophys. Mol. Biol.* **160**, 43–52 (2021).
37. E. Krissinel, K. Henrick, Inference of macromolecular assemblies from crystalline state. *J. Mol. Biol.* **372**, 774–797 (2007).
38. A. J. Pietrzyk, A. Bujacz, J. Mueller-Dieckmann, M. Łochynska, M. Jaskolski, G. Bujacz, Crystallographic identification of an unexpected protein complex in silkworm haemolymph. *Acta Crystallographica Section D: Biological Crystallography* **69**, 2353 (2013).
39. Y. Hou, J. Li, Y. Li, Z. Dong, Q. Xia, Y. A. Yuan, Crystal structure of *Bombyx mori* arylphorins reveals a 3:3 heterohexamer with multiple papain cleavage sites. *Protein Sci.* **23**, 735–746 (2014).
40. K.-S. Ryu, J.-O. Lee, T. H. Kwon, H.-H. Choi, H.-S. Park, S. K. Hwang, Z.-W. Lee, K.-B. Lee, Y. H. Han, Y.-S. Choi, Y. H. Jeon, C. Cheong, S. Kim, The presence of monoglucosylated N196-glycan is important for the structural stability of storage protein, arylphorin. *Biochem. J.* **421**, 87–96 (2009).
41. N. A. Memmel, P. M. Trewitt, K. Grzelak, V. S. Rajaratnam, A. Krishna Kumaran, Nucleotide sequence, structure and developmental regulation of LHP82, a juvenile hormone-suppressible hexamerin gene from the waxmoth, *Galleria mellonella*. *Insect Biochem. Mol. Biol.* **24**, 133–144 (1994).
42. T. Wen, Z. Wang, X. Chen, Y. Ren, X. Lu, Y. Xing, J. Lu, S. Chang, X. Zhang, Y. Shen, X. Yang, Structural basis for activation and allosteric modulation of full-length calcium-sensing receptor. *Sci. Adv.* **7**, eabg1483 (2021).
43. H. Mathys, J. Basquin, S. Ozgur, M. Czarnocki-Cieciura, F. Bonneau, A. Aartse, A. Dziembowski, M. Nowotny, E. Conti, W. Filipowicz, Structural and biochemical insights to the role of the CCR4-NOT complex and DDX6 ATPase in microRNA repression. *Mol. Cell* **54**, 751–765 (2014).
44. M. J. L. J. Fürst, A. Gran-Scheuch, F. S. Aalbers, M. W. Fraaije, Baeyer–Villiger monooxygenases: Tunable oxidative biocatalysts. *ACS Catal.* **9**, 11207–11241 (2019).

45. J. Yan, L. Liang, Q. He, C. Li, F. Xu, J. Sun, E.-B. Goh, N. V. S. N. M. Konda, H. R. Beller, B. A. Simmons, T. R. Pray, V. S. Thompson, S. Singh, N. Sun, Methyl ketones from municipal solid waste blends by one-pot ionic-liquid pretreatment, saccharification, and fermentation. *ChemSusChem* **12**, 4313–4322 (2019).
46. M. Xiong, J. Deng, A. P. Woodruff, M. Zhu, J. Zhou, S. W. Park, H. Li, Y. Fu, K. Zhang, A biocatalytic approach to aliphatic ketones. *Sci. Rep.* **2**, 311 (2012).
47. E. B. Goh, E. E. K. Baidoo, J. D. Keasling, H. R. Beller, Engineering of bacterial methyl ketone synthesis for biofuels. *Appl. Environ. Microbiol.* **78**, 70–80 (2012).
48. T. Burmester, Evolution and function of the insect hexamerins. *Eur. J. Entomol.* **96**, 213–226 (1999).
49. G. Jones, M. Manczak, M. Horn, Hormonal regulation and properties of a new group of basic hemolymph proteins expressed during insect metamorphosis. *J. Biol. Chem.* **268**, 1284–1291 (1993).
50. M. L. Pan, W. H. Telfer, Methionine-rich hexamerin and arylphorin as precursor reservoirs for reproduction and metamorphosis in female luna moths. *Arch. Insect Biochem. Physiol.* **33**, 149–162 (1996).
51. J. Magee, N. Kraynack, H. C. Massey, W. H. Telfer, Properties and significance of a riboflavin-binding hexamerin in the hemolymph of Hyalophora cecropia. *Arch. Insect Biochem. Physiol.* **25**, 137–157 (1994).
52. E. A. Munn, G. D. Greville, The soluble proteins of developing: Calliphora erythrocephala, particularly calliphorin, and similar proteins in other insects. *J. Insect Physiol.* **15**, 1935–1950 (1969).
53. H. Decker, N. Terwilliger, Cops and robbers: Putative evolution of copper oxygen-binding proteins. *J. Exp. Biol.* **203**, 1777–1782 (2000).
54. Y. Li, Y. Wang, H. Jiang, J. Deng, Crystal structure of Manduca sexta prophenoloxidase provides insights into the mechanism of type 3 copper enzymes. *Proc. Natl. Acad. Sci. U.S.A.* **106**, 17002–17006 (2009).
55. A. Lu, Q. Zhang, J. Zhang, B. Yang, K. Wu, W. Xie, Y.-X. Luan, E. Ling, Insect prophenoloxidase: The view beyond immunity. *Front. Physiol.* **5**, 252 (2014).
56. T. Zlateva, P. di Muro, B. Salvato, M. Beltramini, The *o*-diphenol oxidase activity of arthropod hemocyanin. *FEBS Lett.* **384**, 251–254 (1996).
57. H. Decker, T. Rimke, Tarantula hemocyanin shows phenoloxidase activity. *J. Biol. Chem.* **273**, 25889–25892 (1998).
58. B. Salvato, M. Santamaria, M. Beltramini, G. Alzuet, L. Casella, The enzymatic properties of *Octopus vulgaris* hemocyanin: *o*-diphenol oxidase activity. *Biochemistry* **37**, 14065–14077 (1998).
59. T. Nagai, T. Osaki, S. I. Kawabata, Functional conversion of hemocyanin to phenoloxidase by horseshoe crab antimicrobial peptides. *J. Biol. Chem.* **276**, 27166–27170 (2001).
60. T. Masuda, S. Baba, K. Matsuo, S. Ito, B. Mikami, The high-resolution crystal structure of lobster hemocyanin shows its enzymatic capability as a phenoloxidase. *Arch. Biochem. Biophys.* **688**, 108370 (2020).
61. K. Besser, G. P. Malyon, W. S. Eborall, G. Paro da Cunha, J. G. Filgueiras, A. Dowle, L. Cruz Garcia, S. J. Page, R. Dupree, M. Kern, L. D. Gomez, Y. Li, L. Elias, F. Sabbadin, S. E. Mohamad, G. Pesante, C. Steele-King, E. Ribeiro de Azevedo, I. Polikarpov, P. Dupree, S. M. Cragg, N. C. Bruce, S. J. McQueen-Mason, Hemocyanin facilitates lignocellulose digestion by wood-boring marine crustaceans. *Nat. Commun.* **9**, 5125 (2018).
62. H. P. Austin, M. D. Allen, B. S. Donohoe, N. A. Rorrer, F. L. Kearns, R. L. Silveira, B. C. Pollard, G. Dominick, R. Duman, K. el Omari, V. Mykhaylyk, A. Wagner, W. E. Michener, A. Amore, M. S. Skaf, M. F. Crowley, A. W. Thorne, C. W. Johnson, H. L. Woodcock, J. McGeehan, G. T. Beckham, Characterization and engineering of a plastic-degrading aromatic polyesterase. *Proc. Natl. Acad. Sci. U.S.A.* **115**, E4350–E4357 (2018).
63. X. Han, W. Liu, J.-W. Huang, J. Ma, Y. Zheng, T.-P. Ko, L. Xu, Y.-S. Cheng, C.-C. Chen, R.-T. Guo, Structural insight into catalytic mechanism of PET hydrolase. *Nat. Commun.* **8**, 2106 (2017).
64. S. Acebes, F. J. Ruiz-Dueñas, M. Toubes, V. Sáez-Jiménez, M. Pérez-Boada, M. F. Lucas, A. T. Martínez, V. Guallar, Mapping the long-range electron transfer route in ligninolytic peroxidases. *J. Phys. Chem. B* **121**, 3946–3954 (2017).
65. B. C. Knott, E. Erickson, M. D. Allen, J. E. Gado, R. Graham, F. L. Kearns, I. Pardo, E. Topuzlu, J. J. Anderson, H. P. Austin, G. Dominick, C. W. Johnson, N. A. Rorrer, C. J. Szostkiewicz, V. Copié, C. M. Payne, H. L. Woodcock, B. S. Donohoe, G. T. Beckham, J. E. McGeehan, Characterization and engineering of a two-enzyme system for plastics depolymerization. *Proc. Natl. Acad. Sci. U.S.A.* **117**, 25476–25485 (2020).
66. H. Lu, D. J. Diaz, N. J. Czarnecki, C. Zhu, W. Kim, R. Shroff, D. J. Acosta, B. R. Alexander, H. O. Cole, Y. Zhang, N. A. Lynd, A. D. Ellington, H. S. Alper, Machine learning-aided engineering of hydrolases for PET depolymerization. *Nature* **604**, 662–667 (2022).
67. K. Miura, M. Nakagawa, Y. Chinzei, T. Shinoda, E. Nagao, H. Numata, Structural and functional studies on biliverdin-associated cyanoprotein from the bean bug, Riptortus clavatus. *Zool. Sci.* **11**, 537–545 (1994).
68. N. H. Haunerland, W. S. Bowers, Binding of insecticides to lipophorin and arylphorin, two hemolymph proteins ofHeliothis zea. *Arch. Insect Biochem. Physiol.* **3**, 87–96 (1986).
69. K. Wu, J. Zhang, Q. Zhang, S. Zhu, Q. Shao, K. D. Clark, Y. Liu, E. Ling, Plant phenolics are detoxified by prophenoloxidase in the insect gut. *Sci. Rep.* **5**, 16823 (2015).
70. S. H. Scheres, RELION: Implementation of a Bayesian approach to cryo-EM structure determination. *J. Struct. Biol.* **180**, 519–530 (2012).
71. S. Q. Zheng, E. Palovcak, J.-P. Armache, K. A. Verba, Y. Cheng, D. A. Agard, MotionCor2: Anisotropic correction of beam-induced motion for improved cryo-electron microscopy. *Nat. Methods* **14**, 331–332 (2017).
72. K. Zhang, Gctf: Real-time CTF determination and correction. *J. Struct. Biol.* **193**, 1–12 (2016).
73. A. Waterhouse, M. Bertoni, S. Bienert, G. Studer, G. Tauriello, R. Gumienny, F. T. Heer, T. A. P. de Beer, C. Rempfer, L. Bordoli, R. Lepore, T. Schwede SWISS-MODEL: Homology modelling of protein structures and complexes. *Nucleic Acids Res.* **46**, W296–W303 (2018).
74. A. Casañal, B. Lohkamp, P. Emsley, Current developments in Coot for macromolecular model building of Electron Cryo-microscopy and Crystallographic Data. *Protein Sci.* **29**, 1069–1078 (2020).
75. D. Liebschner, P. V. Afonine, M. L. Baker, G. Bunkóczi, V. B. Chen, T. I. Croll, B. Hintze, L. W. Hung, S. Jain, A. J. McCoy, N. W. Moriarty, R. D. Oeffner, B. K. Poon, M. G. Prisant, R. J. Read, J. S. Richardson, D. C. Richardson, M. D. Sammito, O. V. Sobolev, D. H. Stockwell, T. C. Terwilliger, A. G. Urzhumtsev, L. L. Videau, C. J. Williams, P. D. Adams, Macromolecular structure determination using X-rays, neutrons and electrons: Recent developments in Phenix. *Acta Crystallogr. D Struct. Biol.* **75**, 861–877 (2019).
76. E. F. Pettersen, T. D. Goddard, C. C. Huang, E. C. Meng, G. S. Couch, T. I. Croll, J. H. Morris, T. E. Ferrin, UCSF ChimeraX: Structure visualization for researchers, educators, and developers. *Protein Sci.* **30**, 70–82 (2021).
77. W. Kabsch, XDS. *Acta Crystallogr. D Biol. Crystallogr.* **66**, 125–132 (2010).
78. A. J. McCoy, Acknowledging errors: Advanced molecular replacement with phaser. *Methods Mol. Biol.* **1607**, 421–453 (2017).
79. M. Anastassiades, S. J. Lehotay, D. Stajnbaher, F. J. Schenck, Fast and easy multiresidue method employing acetonitrile extraction/partitioning and "dispersive solid-phase extraction" for the determination of pesticide residues in produce. *J. AOAC Int.* **86**, 412–431 (2003).
80. E. Tsochatzis, J. Lopes, H. Gika, G. Theodoridis, Polystyrene biodegradation by *Tenebrio molitor* larvae: Identification of generated substances using a GC-MS untargeted screening method. *Polymer* **13**, 17 (2021).


**Acknowledgments:** We thank the Proteomics and Genomics, Electron Microscopy, and Gas Chromatography facilities of the CIB for the excellent technical support. We acknowledge The Midlands Regional CryoEM Facility at the Leicester Institute of Structural and Chemical Biology (LISCB), major funding from MRC (MC_PC_17136). We thank P. Castroviejo (University of Burgos, Spain) for the excellent technical support in the RAMAN analysis. We thank C. Rovira (University of Barcelona, ICREA-Institució Catalana de Recerca i Estudis Avançats, Spain) for insightful discussion about Cu coordination. **Funding:** This work was funded by Roechling Stiftung to F.B., Consejo Superior de Investigaciones Cientificas (CSIC) to F.B., Ministerio de Ciencia e Innovación (grants PID2019-111215RB-100 and PDC2022-133955-I00) to T.T., Ministerio de Ciencia e Innovación (grant PID2019-111215RB-100) to T.T., the Generalitat de Catalunya (2017 SGR 1192) to M.S., the Spanish Ministry of Science, Innovation and Universities MCIN/AEI/10.13039/501100011033 ERDF "A way to make Europe" PID2021-129038NB-I00 to M.S., and MCIN/AEI/10.13039/501100011033 (grant PID2020-120275GB-I00) to E.A.-P. **Author contributions:** Conceptualization: F.B., C.F.A., E.A.-P., and M.S. Methodology: M.S.-A., R.I.-V., E.R.-L., P.C.-V., F.V.R., R.P.P., C.F.A., T.T., E.A.-P., M.S., and F.B. Investigation: M.S.-A., R.I.-V., E.R.-L., P.C.-V., F.V.R., R.P.P., C.F.A., T.T., E.A.-P., M.S., and F.B. Visualization: M.S.-A., P.C.-V., F.V.R., R.P.P., C.F.A., T.T., E.A.-P., M.S., and F.B. Funding acquisition: F.B., T.T., M.S., and E.A.-P. Project administration: F.B. Writing—original draft: M.S.-A., F.B., C.F.A., E.A.-P., and M.S. Writing—review and editing: M.S.-A., P.C.-V., F.V.R., R.P.P., C.F.A., T.T., E.A.-P., M.S., and F.B. **Competing interests:** Patent application numbers: EP22383172.8 and EP22383174.4. Filing date: 2 December 2022. Authors: F.B., M.S., and E.A.-P. The authors declare no other competing interests. **Data and materials availability:** Cryo-EM maps and atomic coordinates have been deposited in the Electron Microscopy and Protein Data Banks with the following accession numbers: EMD-16521 and PDB ID 8CA9 (Demetra/Cibeles heterocomplex), EMD-16524 and PDB ID 8CAD (Ceres), and EMD-16531 and PDB ID 8CAN (Cora). Coordinates and structure factors of the Cibeles homohexamer solved by x-ray crystallography have been deposited in the Protein Data Bank with accession code PDB ID 8PO9. All data needed to evaluate the conclusions in the paper are present in the paper and/or the Supplementary Materials.

Submitted 17 May 2023
Accepted 15 August 2023
Published 20 September 2023
10.1126/sciadv.adi6813

ScienceAdvances

# Plastic degradation by insect hexamerins: Near-atomic resolution structures of the polyethylene-degrading proteins from the wax worm saliva

Mercedes Spínola-Amilibia, Ramiro Illanes-Vicioso, Elena Ruiz-Lo´pez, Pere Colomer-Vidal, Francisco Ventura Rodriguez, Rosa Peces Pérez, Clemente F. Arias, Tomas Torroba, Maria Sola`, Ernesto Arias-Palomo, and Federica Bertocchini

*Sci. Adv.*, **9** (38), eadi6813.
DOI: 10.1126/sciadv.adi6813







*Science Advances* (ISSN ) is published by the American Association for the Advancement of Science. 1200 New York Avenue NW, Washington, DC 20005. The title *Science Advances* is a registered trademark of AAAS.